Software Contribution

GEOSPHERE

GEOSPHERE, v. 20, no. 3

https://doi.org/10.1130/GES02739.1

6 figures; 2 tables; 2 sets of supplemental files (one set is externally hosted)

CORRESPONDENCE: piercarlo.giacomel@liverpool.ac.uk

CITATION: Giacomel, P., Faulkner, D.R., Lambert, V., and Allen, M.J., 2024, *steadystate*: A MATLAB-based routine for determining steady-state friction conditions in the framework of rate-and-state friction analysis: Geosphere, v. 20, no. 3, p. 965–980, https://doi.org/10.1130/GES02739.1.

Science Editor: Andrea Hampel

Received 27 November 2023
Revision received 5 February 2024
Accepted 1 March 2024

Published online 26 April 2024

steadystate: A MATLAB-based routine for determining steady-state friction conditions in the framework of rate-and-state friction analysis

P. Giacomel[1], D.R. Faulkner[1], V. Lambert[2], and M.J. Allen[1]

[1]Rock Deformation Laboratory, Department of Earth, Ocean and Ecological Sciences, University of Liverpool, Liverpool L69 3GP, UK
[2]Seismology Laboratory, University of California Santa Cruz, Santa Cruz, California 95064, USA

ABSTRACT

Reliable determination of rate-and-state friction (RSF) parameters depends on achieving steady-state (SS) friction conditions before and after experimental velocity-stepping friction tests. This operation, through nonlinear least squares fitting, is commonly preceded by the removal of any overall slip weakening/hardening after friction velocity steps (VSs) through a sufficiently large window of slip displacement at SS (= linear detrend). However, to date, the identification of SS and thus the correct linear detrend is dependent on the user, which potentially results in differing RSF outputs from the same data set. Here, we demonstrate that large errors in the determination of the fitted RSF parameters can result if SS conditions are not reached before and after VSs. Such errors can be particularly relevant for materials characterized by long evolution of frictional resistance with slip, such as clay-rich gouge layers, in which identifying SS after VSs is not always obvious. To this end, we propose a methodology to accurately and consistently identify where SS is achieved after VSs. This methodology is coded into a new MATLAB-based routine, *steadystate*. We show the key features of the methodology, as well as how to use *steadystate* and read its output. We also illustrate the broad applicability of the approach to friction data with different noise levels and sampling frequencies referenced to slip velocity, by reviewing observations from synthetic data sets and specific examples of experiments from different laboratories involving various sheared materials.

1. INTRODUCTION

The rate-and-state friction (RSF) formalism pioneered by J.H. Dieterich, A.L. Ruina, and J.R. Rice (Dieterich, 1979; Rice and Ruina, 1983; Ruina, 1983) has been widely used to understand the processes underlying the spectrum of fault-slip modes exhibited by tectonic faults, i.e., from aseismic to seismic slip, including slow slip behavior (e.g., Ikari, 2019; Leeman et al., 2016, among others). More recently, RSF laws have been applied to a growing number of geomechanical settings and conditions, including catastrophic failure of landslides (e.g., Agliardi et al., 2020; Handwerger et al., 2016; Helmstetter et al., 2004) and glaciers (Hudson et al., 2023; McCarthy et al., 2017; Zoet et al., 2013), as well as a broad range of non-geological materials (Shroff et al., 2014).

To determine the RSF parameters, the most widely used approach consists of running laboratory friction velocity-stepping tests, i.e., friction experiments in which time- and slip-dependent changes in macroscale frictional resistance are monitored through step changes in load-point velocity (Marone, 1998; Scholz, 2019). During the velocity stepping tests, initial steady-state (SS) friction conditions, i.e., constant friction resistance over time and slip preceding the friction velocity steps (VSs), are perturbed, which leads to a step change in frictional resistance, followed by a transient evolution in frictional resistance and consequent attainment of new SS friction conditions at the new slip velocity (Marone, 1998). RSF-dependent constitutive equations specify how frictional resistance varies as a nonlinear function of slip velocity and a set of state variables that describe the material's slip history (see the next section for the functional form of these descriptions). In this framework, RSF parameter values are determined by identifying SS friction conditions before and after VSs, and nonlinear least-squares fitting of the data (Blanpied et al., 1998; Reinen and Weeks, 1993). Before VSs, SS is implicitly assumed (e.g., Giorgetti et al., 2015; Ruggieri et al., 2021), and after VSs, identifying SS can be made more difficult by frictional transients with slip.

A further challenge arises from the superposition of an overall slip dependency in friction (weakening or hardening), which is commonly observed in experimental data sets (e.g., Ito and Ikari, 2015; Kilgore et al., 1993). This type of trend needs to be removed prior to running the inversion scheme. To do this, the most common approach is to select a portion of the friction curve assumed to be at SS conditions, and then use its associated slope to eliminate any average slip-dependent linear trend in friction. This process is known as "linear detrending." Some nonlinear detrending has also been employed (e.g., quadratic detrending; Noda and Shimamoto, 2009), although when using these methods, it is difficult to be certain that SS conditions are

Piercarlo Giacomel https://orcid.org/0000-0002-1553-7842

achieved both before and after VSs, as changes in trend of the friction-versus-displacement curves are typically associated with microstructural changes within the sheared material (e.g., Frank, 1965; Marone et al., 1990). In this study, we only focus on linear detrending. In the vast majority of software programs for determining RSF parameters, points to fit a detrending line are chosen after VSs.

Current practices often rely on the user "eyeballing" when new SS conditions are achieved to perform the detrend procedure or assuming a "standard" value of displacement following the VSs after which SS is assumed. The determination of RSF parameters in such methods is sensitive to how users determine (1) where new SS is reached and (2) the length of the slip window after this point so a linear detrend can be performed to average out experimental noise. This is especially the case in materials characterized by long frictional evolution to the new SS (e.g., Ito and Ikari, 2015). Given such considerations, differing RSF parameters can potentially result from the inversion scheme for the same experimental data set. For example, Skarbek and Savage (2019) pointed out that even small variations in the detrending slope can alter the estimated RSF parameter values. Appropriate identification of SS friction and the correct use of any linear detrend are thus key for reliable determination of RSF parameters and the application of models that depend on these data to characterize earthquake nucleation and fault slip (Dieterich, 1992; Gu et al., 1984; Rubin, 2008). This holds true especially for D_{RS}, which can vary widely upon an incorrect SS assumption and motivates the need to establish consistent and reliable detrending methods for identifying new SS friction conditions and fitting experimental data.

To address the issues identified above, we present a new methodology for determining steady-state conditions that is written as a MATLAB-based routine called *steadystate*. This routine automates the comparison of the slopes estimated by linear regression before and after VSs (termed S1 and S2), with the latter calculated at progressively larger displacements from VSs until new SS conditions are identified, which is defined as when S2 ≈ S1. In particular, the method proposed in this study addresses the issue of finding new SS in VSs characterized by (1) a wide range of noise levels and number of points per unit slip and (2) different average values of slip dependencies in friction superimposed on VSs. To ensure consistency in new SS determination independently of (2), in our routine, estimation of S2 at increasing displacement is preceded by the removal of any average linear trend relative to S1 (provided that S1 ≠ 0), i.e., before VSs. This contrasts from the approach followed in the software currently employed for RSF determination, in which friction data are detrended linearly after VSs.

Previous attempts by the authors to identify SS conditions involved the systematic calculation of the weighted average second derivative of friction with respect to slip, using a tapered, moving slip window, with convergence occurring when the second derivative ≈0 within a tolerance. However, this approach proved less effective in determining the first new SS point after VSs than the method employed in this study, especially in VSs characterized by long frictional evolution to the new SS.

TABLE 1. LIST OF FREQUENTLY USED SYMBOLS AND ABBREVIATIONS

Symbol	Description
RSF	Rate-and-state friction
SS	Steady-state friction
VS	Friction velocity step
a	Direct effect (RSF parameter)
b_i	Evolution effect (RSF parameter) relative to the i-th state variable
D_{RSi}	Characteristic slip distance (RSF parameter) relative to the i-th state variable
a-Σb_i	Friction velocity dependence (RSF parameter) under steady-state conditions
k'	Elastic stiffness of the system normalized to the normal stress (1/μm)
S1	Slope measured before the velocity steps via linear regression (1/μm)
L_{S1}	Slip window length for the linear regression to get S1 (μm)
S2	Slope measured after the velocity steps via linear regression (1/μm)
|S2|	Absolute value of S2
L_{S2}	Slip window length for the linear regression to get S2 (μm)
min_L_{S2}	Minimum L_{S2} used to estimate S2 in steadystate.m (automatic input by default or entered by the user) (μm)
max_L_{S2}	Maximum L_{S2} used to estimate S2 in steadystate.m (automatic input by default or entered by the user) (μm)
ΔL_{S2}	Interval in L_{S2} used to estimate S2 in steadystate.m (automatic input by default or entered by the user) (μm)
$\Delta\delta$	Displacement interval from an S2 measurement to the next one using a given L_{S2} in steadystate.m (automatic input by default or entered by the user) (μm)
f	Sampling frequency (Hz)
V	Slip velocity (μm/s)
N_{norm}	Number of points per unit of slip (1/μm) = f/V
SD	Standard deviation of the random Gaussian noise superimposed to the synthetic velocity steps
RMSE	Root mean squared error of the linear regression
TH10	Threshold in |S2| ensuring modelled RSF parameters within 10% error relative to the intrinsic RSF values (1/μm)
δ_{TH10}	Displacement at which the condition TH10 is first met (1/μm) after the velocity steps

In the following sections, we give the background details on the RSF framework (section 2), then describe the RSF analysis of synthetic velocity steps including the methodology employed in *steadystate* (section 3). This is followed by applications of the SS analysis to both synthetic and experimental VSs (section 4), and the workflow illustrating the main architecture of the code (section 5). For the complete list of symbols and abbreviations used, refer to Table 1. *steadystate* is available on Github (https://github.com/pgiacomel/steadystate).

2. BACKGROUND

In laboratory friction data, the frictional resistance (μ) is determined as the ratio between the macroscopic shear resistance (τ) at the sliding

interface or within the volume of powdered material, and the effective normal stress acting on the sample (σ'_n), which is commonly quantified using the effective stress law $\sigma'_n = \sigma_n - P_f$ (Terzaghi, 1925), where σ_n and P_f are the applied normal stress and pore fluid pressure, respectively. Empirical RSF laws postulate that the change in frictional resistance (μ) to a sudden change in load point velocity can be described as a function of slip velocity (V) and a set of state variables (θ_i), whose number (i) is dependent on the friction data being fit.

Equation 1 represents the two-state variable form of the Dieterich-Ruina constitutive equation (Dieterich, 1979; Ruina, 1983):

$$\frac{\tau}{\sigma'_n} = \mu(V,\theta) = \mu_0 + a\ln\frac{V}{V_0} + b_1\ln\left(\frac{V_0\theta_1}{D_{RS1}}\right) + b_2\ln\left(\frac{V_0\theta_2}{D_{RS2}}\right), \quad (1)$$

where a, b_1, and b_2 are dimensionless, empirically derived constants (with $b = b_1 + b_2$), and V_0 and V are the load point velocities before and after the VS, respectively. We prefer the use of D_{RS} to describe the characteristic slip distance rather than D_c as often denoted in RSF studies to avoid any ambiguity with the critical slip distances used for linear slip-weakening friction laws (Dal Zilio et al., 2022; Erickson et al., 2023; Lambert et al., 2021). The first term on the right side of Equation 1, μ_0, is the reference SS friction coefficient determined at V_0; the second term represents the direct effect, i.e., the direct friction response to the step change in load point velocity until the achievement of a peak value, which is scaled by a. In an infinitely stiff apparatus, the local maximum (or minimum) in friction is reached immediately following the VS. The third and fourth terms represent two separate contributions to the evolution effect, which describes the evolution of the friction coefficient with slip to a new SS following a VS. The evolution terms in Equation 1 are scaled by b_i, and evolve with characteristic slip distances, D_{RSi}. Because the characteristic slip distance relates to the slip necessary to effect a change from one SS friction value to another after a slip-velocity perturbation, its magnitude clearly affects the cumulative shear displacement at which new SS conditions are reached. In the laboratory, materials typically display D_{RS} of ~10 µm, but in a few cases, such as in clay-rich materials, D_{RS} can reach values of ~100 µm or greater (e.g., Ikari, 2019; Ikari and Hüpers, 2021; Ito and Ikari, 2015; Niemeijer et al., 2010; Pozzi et al., 2023; Sawai et al., 2016). D_{RSi} scales the evolution of the state variables, θ_i, which reflect slip-history effects with units of time, and are often conceptualized in terms of the average lifetime of load-bearing contacts during frictional sliding (Dieterich, 1979, 1981; Dieterich and Conrad, 1984) or as contact strength (Goldsby et al., 2004; Nakatani, 2001; Thom et al., 2023).

The two most widely employed mathematical descriptions of the time- (and slip-) dependent evolution of the state variables upon a step change in load point velocity are the aging law (Equation 2A; Dieterich, 1979) and the slip law (Equation 2B; Ruina, 1983):

$$\frac{d\theta_i}{dt} = 1 - \frac{V\theta_i}{D_{RSi}},\ i = 1,2, \quad (2A)$$

$$\frac{d\theta_i}{dt} = -\frac{V\theta_i}{D_{RSi}}\ln\left(\frac{V\theta_i}{D_{RSi}}\right),\ i = 1,2. \quad (2B)$$

Note that at SS friction conditions, $d\theta_i/dt = 0$, and consequently, both state evolution laws yield $\theta_{ssi} = D_{RSi}/V$. Substituting this into Equation 1 quantifies the velocity dependence of friction under SS sliding conditions:

$$a - b = a - \Sigma b_i = \frac{\Delta\mu_{ss}}{\ln\frac{V}{V_0}}, \quad (3)$$

where $\Delta\mu_{ss}$ is the SS change in friction following a step change in slip velocity from V_0 to V. Within this framework, positive values of $a - b$ define the SS friction-velocity strengthening behavior associated with stable frictional sliding, whereas if $a - b < 0$, friction is SS velocity weakening, which is a requirement for the onset of unstable slip.

To evaluate whether materials exhibiting SS velocity weakening display dynamic slip, a single degree of freedom spring-slider system is introduced (e.g., Cook, 1981; Gu et al., 1984; Ruina, 1983). Although it is a simplified representation, the 1-D spring-slider system reasonably describes in the laboratory the interplay between the frictional properties of the surface/gouge layer and the elastic stiffness of the surroundings in terms of time derivative of the shear resistance τ, such that:

$$\frac{d\tau}{dt} = k\left(v_{lp} - v\right), \quad (4)$$

where v_{lp} is the load point velocity, v is the frictional sliding velocity resolved at the surface interface/gouge layer, and k is the elastic loading stiffness of the system (measured in unit stress/unit length). Assuming constant effective normal stress, σ'_n throughout the test, Equation 4 can be rewritten as the first derivative in time of the friction coefficient, with $k' = k/\sigma'_n$ (given in 1/unit of length).

Friction stability analysis (Gu et al., 1984) and the estimation of the minimum patch size for the nucleation of frictional instabilities (Rubin, 2008; Rubin and Ampuero, 2005) rely on the correct determination of the friction velocity dependence *(a–b)* and of D_{RS}. To extract the constitutive parameters a, b_i, and D_{RSi} from friction data sets, the coupled Equations 1, 2A or 2B, and 4 are solved, and a nonlinear least squares routine is employed to find the optimum fit of the RSF parameters. Cases in which RSF fit converges with $D_{RS1} \approx D_{RS2}$ or $b_2 = 0$ indicate that a single-state variable constitutive law is sufficient to adequately model the data (e.g., Marone and Cox, 1994).

A detailed explanation of the iterative least squares method employed to solve the inverse problem is described in the papers of Bhattacharya et al. (2015), Blanpied et al. (1998), and Reinen and Weeks (1993). Such inversion schemes are incorporated into the software programs that are commonly used to determine RSF parameters, which include, among others, (1) xlook (https://github.com/PennStateRockandSedimentMechanics/xlook); (2) versions developed in Jupiter Notebook/python's environment based on the xlook tool, such as rawPy (https://github.com/marcoscuderi/rawPy); (3) the codes of Bhattacharya et al.

(2015) using Fortran, which are available at https://zenodo.org/record/2631455; and (4) the latest release using a MATLAB-based GUI, RSFit3000, which can be found on Github (https://github.com/rmskarbek/RSFit3000) and in Skarbek and Savage (2019). As the stiffness of the system can vary by >50% during shearing in a friction test (Leeman et al., 2016; Scuderi et al., 2017), k is often used as a fitting parameter during the numerical inversions (Noda and Shimamoto, 2009).

The determination of the fitting parameters is preceded by the removal of any linear slip-dependence in friction at SS conditions following the velocity steps:

$$\mu' = \mu + m[\delta_{ref} - \delta(t)], \quad (5)$$

in which μ' and μ are the linear detrended and experimental (i.e., undetrended) friction values pertaining to the selected VSs, δ_{ref} is the displacement reference value where the velocity jump occurs, and $\delta(t)$ is the slip accumulated with time during the velocity step test. m refers to the slope calculated via linear regression within a slip window of an arbitrary length, and represents the magnitude of the average linear friction slip dependence that is removed from the friction curve μ to obtain μ'.

3. A GENERAL CRITERION FOR DETERMINING STEADY STATE

To investigate the effects of incorrect assumptions of SS friction conditions on the determination of RSF parameters and to develop an unbiased methodology for determining new SS, synthetic VSs from V_1 = 0.3 to V_2 = 3 µm/s were generated using a single degree of freedom spring-slider system (Equation 4), via the RSF constitutive law described by two sets of state variables (Equation 1) coupled with the "slip" evolution law (Equation 2B). In this study, synthetic VSs mimic experimental data sampled at a frequency of f = 100 Hz and with a random Gaussian noise of standard deviation SD = 0.0005 added to each data point to simulate the electrical noise (e.g., Chartrand, 2011; Skarbek and Savage, 2019). Friction is at SS conditions before VSs, and no slip dependencies in friction have been superimposed. The slope associated with the friction data preceding VSs (S1) is ≈0 when using a slip window length of 200 µm for the linear regression (-1.38×10^{-8} µm^{-1}). S1 ≈ 0 is a sine qua non for applying the procedures described for determining steady-state, as it removes one variable from the system. Note that S1 = 0 occurs only in unrealistic zero-noise scenarios.

VSs were produced for D_{RS2} = 0 – 50 – 100 – 200 – 500 µm, and run for step lengths of 3 mm in the D_{RS2} = 500 µm step test and 2 mm in the remainder of the tests. Such step lengths are greater than those usually documented in the geomechanical literature to ensure that SS at the new slip velocity is reached. To mimic the elastic loading stiffness for biaxial (e.g., Collettini et al., 2014; Leeman et al., 2016; Scuderi et al., 2017) and triaxial deformation apparatuses (e.g., Bedford et al., 2021; Faulkner et al., 2018), k' = 0.01 and 0.001 µm^{-1} were used, respectively. The sets of parameter values used to generate synthetic VSs are included in Table 2. Their relative VSs are displayed in Figure S1[1] and stored in the externally hosted files.[2]

For all VSs, the first new SS candidate point was chosen at 200 µm after the VS to account for the effects that could occur in compliant deformation apparatuses following the velocity jump, such as upstep-induced friction oscillations (e.g., Gu et al., 1984) or a long direct effect. Then, a slip window with a constant length of 100 µm was used from the selected point onwards to linearly detrend the friction data (Equation 5) using the slope S2. All friction points following the slip window used for detrending were neglected. Following the detrend, the RSF fitted parameters were determined using one-state and two-state variable fits and compared with the intrinsic parameters used to generate VSs. The same operation was repeated but with a slip window that was shifted forward by 100 µm until the end of the data was reached. During each RSF fit, the detrending slope S2 was systematically compared with S1.

Figure 1 illustrates the VS with intrinsic D_{RS2} = 500 µm and k' = 0.01 µm^{-1}, and highlights two examples of SS analysis carried out at a small displacement (linear detrend between 400 µm and 500 µm: panel I, red dashed rectangle, Figs. 1A and 1B) and at a large displacement (linear detrend between 2300 µm and 2400 µm: panel II, green dashed rectangle, Figs. 1A and 1C) following the VS. The complete collection of RSF values obtained by detrending friction data at increasing displacements is reported in Figure 2 and stored in the externally hosted supplemental files (see footnote 2). In Figures 2A and 2B, fitted RSF parameters are normalized by the intrinsic RSF values, so that when normalized data approach unity, fitted and intrinsic RSF parameters essentially coincide. Data are plotted as a function of their associated detrending slopes |S2| (shown by the color bar in Fig. 2). The friction velocity dependence a–Σb in Figure 2C corresponds to a–b and a–b_1–b_2 when friction data are modeled using a one-state and two-state variable fit, respectively; analogously, modeled D_{RS} in Figure 2D refers to D_{RS} for the one-state and D_{RS2} for the two-state variable case. For a direct comparison with fitted data, the intrinsic RSF parameters relative to the friction velocity dependence and D_{RS} are also shown (light blue lines in Figs. 2C and 2D).

Overall, results from Figures 1 and 2 elucidate significant differences in RSF parameters resulting from incorrectly choosing SS in different parts of the datafile, as well as assuming a one-state variable fit to data when a two-state variable fit is more appropriate. Non-SS conditions are associated with a discernible slope before the VS following the detrending operation, so that S1 becomes different than zero (Fig. 1D). This is a feature commonly seen in experimental data sets. Conversely, when |S2| ≈ S1 ≈ 0, SS conditions are reached, and modeled RSF values approach the intrinsic RSF parameters (Figs. 1E, 2A, and 2B).

[1]Supplemental Material. Figures S1–S5. Please visit https://doi.org/10.1130/GEOS.S.25456102 to access the supplemental material, and contact editing@geosociety.org with any questions.

[2]Supplemental Material (externally hosted). Dataset and MATLAB scripts to generate the figures related to this article. Please visit https://doi.org/10.5285/0a6b0b0c-b84e-44fd-a331-7c1b4ff9165e in the BGS National Geoscience Data Centre under the Open Government Licence (ID 184041).

TABLE 2. LIST OF SYNTHETIC VELOCITY STEPS

Simulated material properties							Applied conditions					Figure	Section
μ_0	Intrinsic rate-and-state friction parameters												
	a	b_1	b_2	D_{RS1} (μm)	D_{RS2} (μm)	k′ (μm^{-1})	V_1 (μm/s)	V_2 (μm/s)	δ_{ref} (μm)	Step length (μm)	Noise SD	f (Hz)		
0.6	0.012	0.01	0.007	20	0	0.01	0.3	3	200	2000	0.0005	100	S1a	3
0.6	0.012	0.01	0.007	20	50	0.01	0.3	3	200	2000	0.0005	100	S1b	3
0.6	0.012	0.01	0.007	20	100	0.01	0.3	3	200	2000	0.0005	100	S1c	3
0.6	0.012	0.01	0.007	20	200	0.01	0.3	3	200	2000	0.0005	100	S1d	3
0.6	0.012	0.01	0.007	20	500	0.01	0.3	3	200	3000	0.0005	100	1, S1e	3,4
0.6	0.012	0.01	0.007	20	500	0.001	0.3	3	200	3000	0.0005	100	S1f	3
0.6	0.012	0.01	0.007	20	500	0.01	0.3	3	200	3000	0.0005	1	S1g	4
0.6	0.012	0.01	0.007	20	500	0.01	0.3	3	200	3000	0.0005	10	S1h	4
0.6	0.012	0.01	0.007	20	500	0.01	0.3	3	200	3000	0.0005	1000	S1i	4
0.6	0.012	0.01	0.007	20	500	0.01	0.3	3	200	3000	0.00025	1	S1j	4
0.6	0.012	0.01	0.007	20	500	0.01	0.3	3	200	3000	0.00025	10	S1k	4
0.6	0.012	0.01	0.007	20	500	0.01	0.3	3	200	3000	0.00025	100	S1l	4
0.6	0.012	0.01	0.007	20	500	0.01	0.3	3	200	3000	0.00025	1000	S1m	4
0.6	0.012	0.01	0.007	20	500	0.01	0.3	3	200	3000	0.01	1	S1n	4
0.6	0.012	0.01	0.007	20	500	0.01	0.3	3	200	3000	0.01	10	S1o	4
0.6	0.012	0.01	0.007	20	500	0.01	0.3	3	200	3000	0.01	100	S1p	4
0.6	0.012	0.01	0.007	20	500	0.01	0.3	3	200	3000	0.01	1000	S1q	4

Notes: List of synthetic velocity steps generated obeying the rate-and-state constitutive law with two-state variables, coupled with the "slip" state variable evolution law, using a one-dimensional spring-slider model as a constraint. μ_0—reference steady-state friction coefficient before the velocity step; k′—elastic stiffness of the simulated system; V_1—slip velocity prior to the velocity step; V_2—slip velocity after the velocity step; step length—step length (after the velocity step); δ_{ref}—reference displacement after which the velocity step occurs (numerically equivalent to the slip accumulated before the velocity step); SD—standard deviation relative to the Gaussian noise superimposed to the synthetic velocity step; f—sampling frequency of the data file.

Our data notably show that the earlier new SS is assumed within the non-SS stages of the frictional transients following a VS, the more the detrending operation can produce misleading interpretations of the friction velocity dependence, as in Figure 1B. Under such circumstances, apparent velocity strengthening can be observed even in inherently strong velocity-weakening materials, for both one- and two-state variable fits (Fig. 2C), with D_{RS2} significantly underestimated (Fig. 2D). This effect is exacerbated at higher intrinsic D_{RS2} (Figs. 3A, 3B, and S2; see footnote 1), which testifies that the correct determination of SS becomes a more prominent issue the longer the frictional transients with slip are.

It is interesting to note that when friction data are fitted using a two-state variable constitutive law, the modeled direct effect, a, and the parameters related to the first-state variable (b_1 and D_{RS1}) map onto the intrinsic RSF parameters used to generate the synthetic VSs regardless of |S2|, and thereby, of the displacement at which new SS is assumed (Fig. 2A). Conversely, the parameters related to the second-state variable (b_2 and D_{RS2}) are very sensitive to variations in the new SS choice and tend to be their true values when new SS is assumed at larger displacements, where $|S2| \approx S1 \approx 0$ (Figs. 2C and 2D). This is due to the progressive incorporation of the longer evolution effect relative to the second-state variable while fitting the friction event. Equivalent conclusions are also drawn for the VS with $k = 0.001$ μm^{-1} (Figs. S1F, S3, and S4; see footnote 1), which illustrates that the same approach can be followed for a wide range of machine stiffnesses employed for assessing the frictional stability in the laboratory.

Building on the above observations, the systematic determination of |S2| and its comparison with S1 along VSs can be employed in automated routines as a method to ensure the correct determination of a new SS condition, which is associated with |S2| approaching 0 during shearing in all VSs characterized by $S1 \approx 0$. However, since this condition is met asymptotically (Figs. 2C and 2D), it is useful to define a threshold for |S2| below which new SS is assumed in the routine *steadystate*. Called TH10, this threshold is defined from the synthetic VS depicted in Figure 1 (i.e., with $D_{RS2} = 500$ um) as $|S2| = 5 \times 10^{-7}$ μm^{-1}, and results in less than ±10% error in the recovered parameters compared with the intrinsic RSF values (shaded gray areas in Figs. 2 and 3A). Figures 2C and 2D notably highlight the $(a–b_1–b_2)$ and D_{RS2} parameter values from the modeled data used to constrain TH10 (red-bordered triangle).

Modeling friction data obeying a two-state variable constitutive law with a single set of state variables may, in some cases, return erroneous RSF parameters even when new SS is correctly determined (Fig. 2B). This holds true especially for modeled D_{RS} values (Fig. 2D) in steps with long evolution effects (Fig. 3B), although at SS, the friction velocity dependence $(a–b)$ is still well

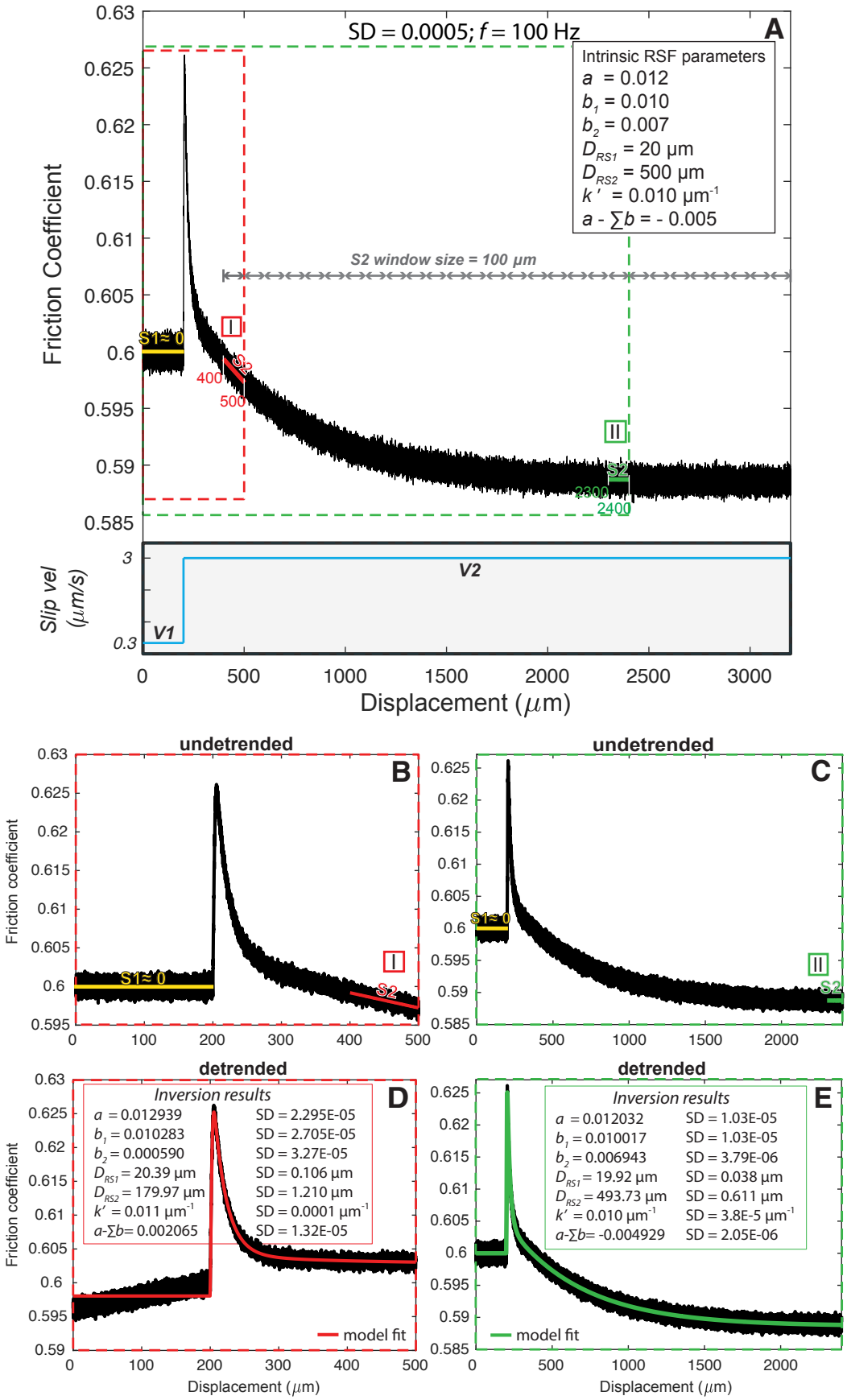

Figure 1. (A) Illustration of a synthetic friction velocity step (VS) generated at a sampling rate of 100 Hz using two-state variables and superimposed with a random Gaussian noise with a standard deviation (SD) of 0.0005. The intrinsic rate-and-state friction (RSF) parameters used to generate VS are outlined in part A. Before VS, slope S1 ≈ 0. S2 represents the 100-μm-long average slope of friction with slip located after VS that is removed prior to determining RSF parameters; this operation is reiterated by shifting the regression line of 100 μm toward larger displacements. Panel I denotes the first analysis with |S2| >> 0, whereas II shows a case in which |S2| ≈ 0. (B and C) Magnification of panels I and II, respectively; (D and E) their corresponding detrended VS, and the associated fitted parameter values.

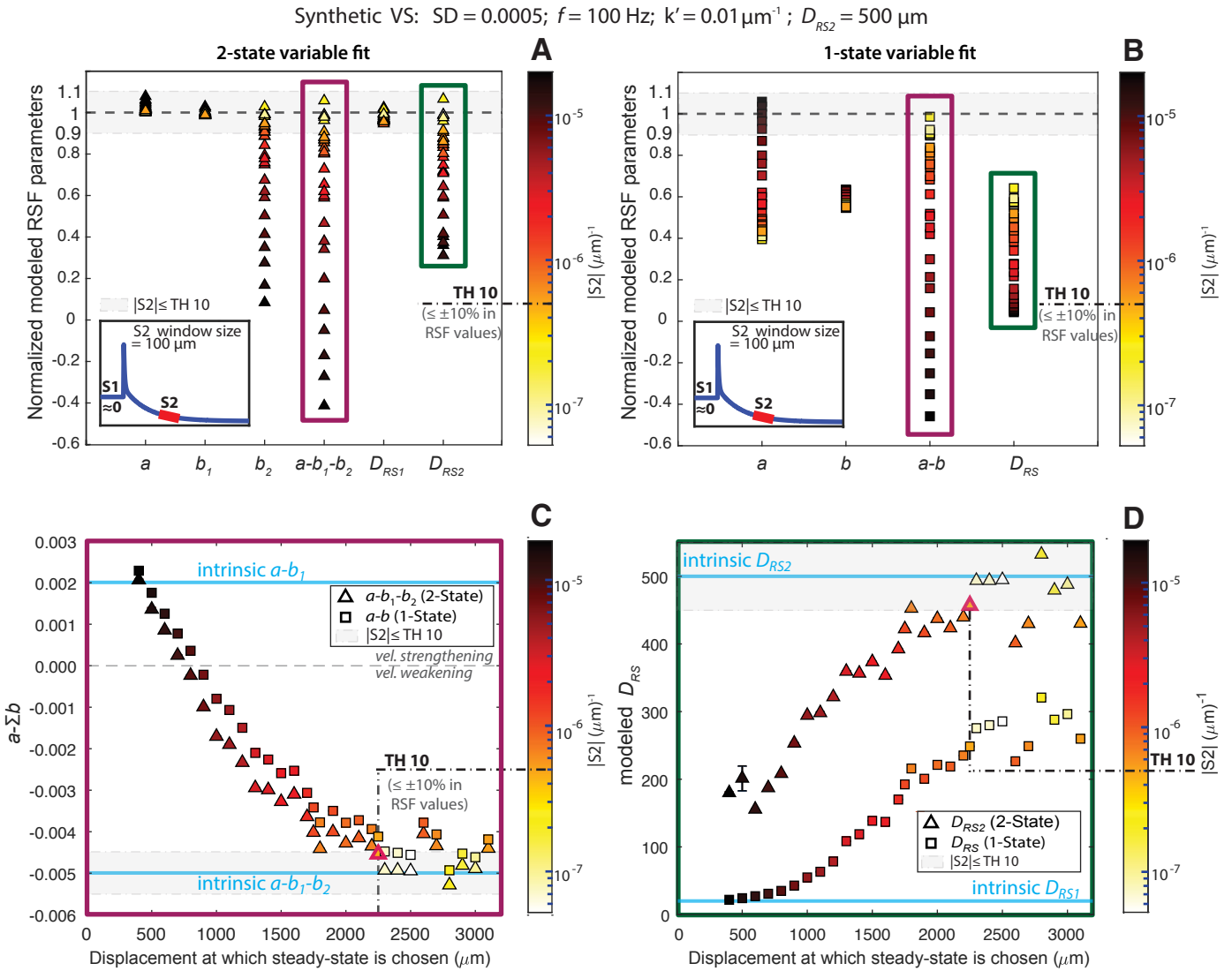

Figure 2. (A and B) Collection of rate-and-state friction (RSF) parameter values obtained after systematically removing the detrending slope S2 along the synthetic velocity step of Figure 1 at progressively larger displacements after the step change in slip velocity, using (A) a two-state variable fit, and (B) a one-state variable fit. The parameters are normalized by the intrinsic RSF values and plotted as function of the module of S2, |S2| (color coded). Grey shading indicates the region characterized by fitted RSF parameters that differ from the intrinsic values by ± 10% or less. TH10 is the threshold in |S2| that allows determination of RSF parameters within the gray shaded region when using the velocity step of Figure 1. (C) Modeled *a*–Σ*b* and (D) D_{RS} using a two-state variable fit and a one-state variable fit (contained in red and green rectangles in parts A and B, respectively) are plotted against the displacement at which steady-state is chosen and the detrending slope S2 applied. For comparison, the intrinsic friction velocity dependence $a–b_1–b_2$ and $a–b_1$, as well as D_{RS1} and D_{RS2}, are also shown (light blue lines). SD—standard deviation. vel.—velocity.

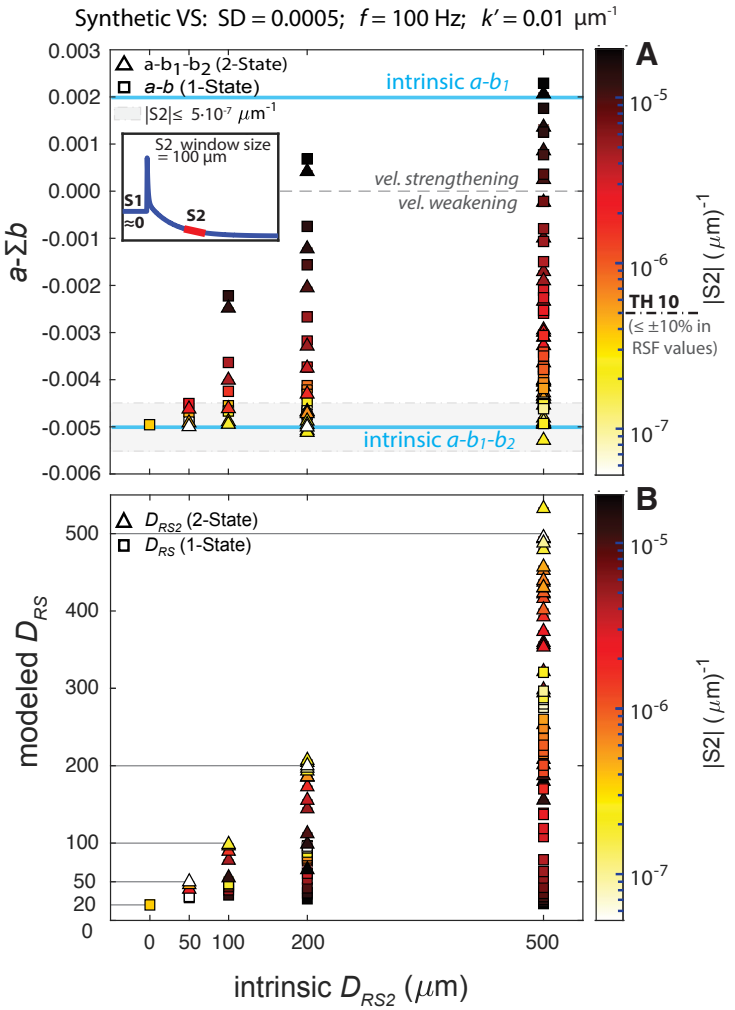

Figure 3. Data set obtained from synthetic velocity steps with the same rate-and-state friction (RSF) parameter values (a = 0.012; b_1 = 0.010; D_{RS1} = 20 μm ; k′ = 0.01 μm^{-1}) except for the intrinsic D_{RS2} spanning from 0 μm to 500 μm. (A) Fitted a–Σb values and (B) D_{RS} are shown as a function of the intrinsic D_{RS2} and the absolute value of S2, |S2| (color coded). Points in the graph represent all fitted parameter values retrieved using a two-state and one-state variable fit, following the linear detrend operated at increasing displacements by estimating S2 through a 100-μm-long slip window. TH10 is the threshold in |S2| (= 5·10^{-7} μm^{-1}) determined from a velocity step with intrinsic D_{RS2} of 500 μm, which allows determination of fitted RSF parameters within the ± 10% error relative to the intrinsic RSF parameter values; the lower the intrinsic D_{RS2}, the larger the tolerance in |S2| estimation for pinpointing new steady-state conditions, and hence the likelihood of obtaining RSF parameters close to the intrinsic parameters. SD—standard deviation. vel.—velocity.

described (Figs. 2B, 2C, and 3A). Therefore, our data suggest that, after determining the first point at new SS conditions and detrending the data, it is good practice to begin the inversion scheme with a two-state variable model and consider a single-state variable fit only as a follow-up stage.

4. KEY FACTORS INFLUENCING STEADY-STATE DETERMINATION

When applying the approach in section 3, determination of SS relies on the accuracy of the slope estimation before and after the VSs via linear regression analyses (i.e., S1 and S2, Figs. 1 and S3). Slope calculations can be influenced by the combination of the level of noise of the friction data and the number of datapoints used for the linear regression.

The closest approximation to the noise characterizing electric signals is the random Gaussian noise, which is quantified by its standard deviation (SD). Several factors contribute to the average noise in friction experimental data, including the apparatus, the applied effective normal stress, and the environment (e.g., presence of electronic devices interfering with the electric signal from transducers). The number of points per unit slip, N_{norm}, relates the sampling frequency, f, to the slip velocity, V, as $N_{norm} = f/V$.

To investigate the effect of noise and number of datapoints used to determine SS, the methodology described in section 3 was automated through the MATLAB routine *steadystate*. To investigate how we could minimize the effect of noise and sampling frequency, we also varied the length of the window (L_{S2}) in units of displacement from 50 μm to 500 μm with increments of 50 μm. A key difference between the manual and automated methodology is that in the latter, SS is chosen on the basis of |S2| falling below the threshold formerly defined (see section 3) as TH10 = 5 × 10^{-7} μm^{-1} rather than identifying δ_{TH10}, which is the displacement at which the error in the returned rate and state parameters falls below ±10%. Clearly, when real experimental data are used, the intrinsic rate and state parameters are unknown, and hence δ_{TH10} cannot be determined, so this alternate approach is necessary in the automated routine *steadystate*.

steadystate was applied to the same synthetic VS as in Figure 1, but with a broader range of random Gaussian noise and sampling frequencies applied. Three levels of noise were analyzed with various SDs: (1) 0.00025 (low noise), (2) 0.0005 (intermediate noise), and (3) 0.001 (high noise). The sampling frequency was varied from 1 Hz to 1000 Hz, with f increasing log-linearly from one test to another. The wide spectrum of SD and N_{norm} used in this study encompasses, to the best of our knowledge, the vast majority of the values that can be found in velocity-stepping experiments within laboratories worldwide.

S1 was determined over a 200 μm slip window before the velocity jump occurred, which ensures S1 ≈ 0 over the investigated range of SD and N_{norm}. As with the analysis in the previous section, the first new SS candidate point is chosen at 200 μm slip after the VS, and the slip window of length L_{S2} is moved to higher displacements by 100 μm increments until the new SS condition is

met. The first new SS points compiled, obtained using the criterion $|S2| \leq 5 \times 10^{-7}$ μm^{-1}, are plotted against the slip-window length used (L_{S2}; Fig. 4), and collected in the externally hosted supplemental files (see footnote 2).

Also included in Figure 4 for comparison is the displacement at which new SS was chosen via the criterion δ_{TH10} described in section 3 (which produces modeled RSF parameters within ±10% of the intrinsic values). The two analyses, based on the criteria $|S2| \leq 5 \times 10^{-7}$ μm^{-1} and δ_{TH10}, produce comparable results in terms of first new SS points (red-edged triangle versus δ_{TH10}, Fig. 4B). The displacements associated with SS that ensure fitted RSF parameters within ± 20%, 40%, and 65% of the intrinsic values are also reported (i.e., δ_{TH20}, δ_{TH40}, and δ_{TH65}, black dashed lines in Fig. 4). The error lines can be a proxy for the goodness of SS determination as a function of data noise, number of points per unit slip, and S2 window length L_{S2}, in VSs processed with *steadystate*.

Overall, our data in Figure 4 confirm that combinations of noisy data (large SD) and a small number of data points (resulting from small N_{norm} and/or small L_{S2}) produce poor linear regressions for estimating S2, and thus erratic new SS determinations. This can be ascribed to the presence of influential points introduced by the superimposed noise, which becomes more relevant the fewer the number of points. Consequently, new SS outputs characterized by significant dependencies in L_{S2} (e.g., purple squares at $L_{S2} \leq 200$ μm in Figs. 4B and 4C), in addition to those falling below the region delimited by δ_{TH20} (e.g., purple squares at $L_{S2} < 200$ μm in Fig. 4A), are likely affected by poor S2 determination, and are therefore unreliable.

A solution to these issues (at a given noise level, sampling rate, and slip velocity) would be to increase L_{S2}, so that the points inducing such issues become less influential in the slope estimation, leading to a more accurate new SS determination (Hastie et al., 2009; James et al., 2013). If a sufficiently large L_{S2} is chosen, whose length depends on SD (e.g., comparison of green triangles in Figs. 4A–4C) and N_{norm} (e.g., Fig. 4A), the analysis generates approximately the same choice of displacement value related to new SS for progressively larger L_{S2} (Figs. 4 and S5B; see footnote 1).

For efficiency reasons, and because slip windows are commonly short in experimental data, the routine identifies the first new SS point with the smallest L_{S2} associated with the constant portion of the plot (i.e., "optimum" output, red-bordered dot, Figs. 5 and 6I; see section 5.4, phase 3, for details).

Examples of the application of *steadystate* to experimental VSs are reported in Figure 5. These case studies illustrate the broad applicability of the routine *steadystate* to friction data from different laboratories, characterized by different machine stiffnesses, noise levels, average friction slip dependencies, and sheared materials with various RSF properties (Figs. 5A and 5B). Materials characterized by long frictional transients with slip, hence large D_{RS} (e.g., clay-rich sepiolite gouge from Sánchez-Roa et al., 2016, 2017; Figs. 5B, 5D, and S5A), require larger displacements to reach new SS conditions when compared to the step length of 500 μm that is typically used in velocity-stepping tests (Figs. 5F and S5B). Conversely, in materials with short frictional evolution with slip (e.g., unaltered basalt gouge from Giacomel et al., 2021; Figs. 5A and 5C), a VS length of 500 μm is typically sufficient to attain new SS (Fig. 5E).

5. WORKFLOW

In this section, we outline the workflow used in *steadystate*. The routine follows the work protocol described in section 3, and finds its basis for the new SS determination in the key findings of the previous sections.

5.1 Phase 0: Slicing Velocity Steps and Selecting Points

The first preliminary operation is to slice the velocity-stepping experiment into its single VSs (phase 0, Fig. 6). One way to do so is via *slicing_velsteps*, i.e., a standalone script containing step-by-step instructions to follow in the MATLAB Command Window, which allows the whole spectrum of mechanical datafiles from worldwide rock deformation laboratories to be read and sliced. In doing so, friction-versus-displacement and friction-versus-time curves relative to each sliced velocity-stepping friction test are automatically displayed, and their corresponding data, including the effective normal stress, are stored in .txt format. Once the VSs are properly sliced, the main routine *steadystate* is ready to be run. In the first stage of *steadystate*, for each VS the user needs to select, in consecutive order, the three main points required for the new SS assessment, namely: (1) the first point of the analysis before the VS where SS has been established; (2) the reference point, ref, at which the VS occurs; and (3) the end of the datafile after slicing (i.e., the last point where the slope S2 can be estimated). Figure 6B illustrates an example of data-point selection preceding the SS analysis.

5.2 Phase 1: Preliminary Removal of S1 Slope

The automatization of the protocol outlined in section 3 requires S1 to be quantified before S2 is estimated, so the average slope before the VSs can be removed to begin the SS assessment with $S1 \approx 0$ as a starting condition (phase 1, Fig. 6). This operation allows determination of the new SS in a consistent manner, as the same threshold value for slope S2 (i.e., TH10, section 3; Fig. 2) would be used for all VSs. Since the condition $S1 = 0$ cannot be reached in experimental data and the criterion for new SS is $|S2| \approx S1$ (Fig. 1C) with $|S2| \leq TH10 = 5 \times 10^{-7}$ μm^{-1} when $S1 \rightarrow 0$ (Fig. 2), the value at which S1 can be reasonably considered ≈0 has been set to the same value previously determined for S2, i.e., $|S1| \leq TH10$. Therefore, in the event $|S1| > 5 \times 10^{-7}$ μm^{-1} (Fig. 6D), the average linear friction slip dependence before the VS is removed from the entire friction event (Equation 5; Figs. 6E and 6F). Note that this procedure is applied only internally in the routine, without modifying the output friction data that appear in MATLAB workspace after the analysis.

S1 is calculated from the linear regression of friction-versus-displacement data between points 1 and 2 (Fig. 6B). To deal with the issues of noise and/or small numbers of data points for S1 determination, we determine the average noise level and N_{norm} from the experimental friction data between the selected

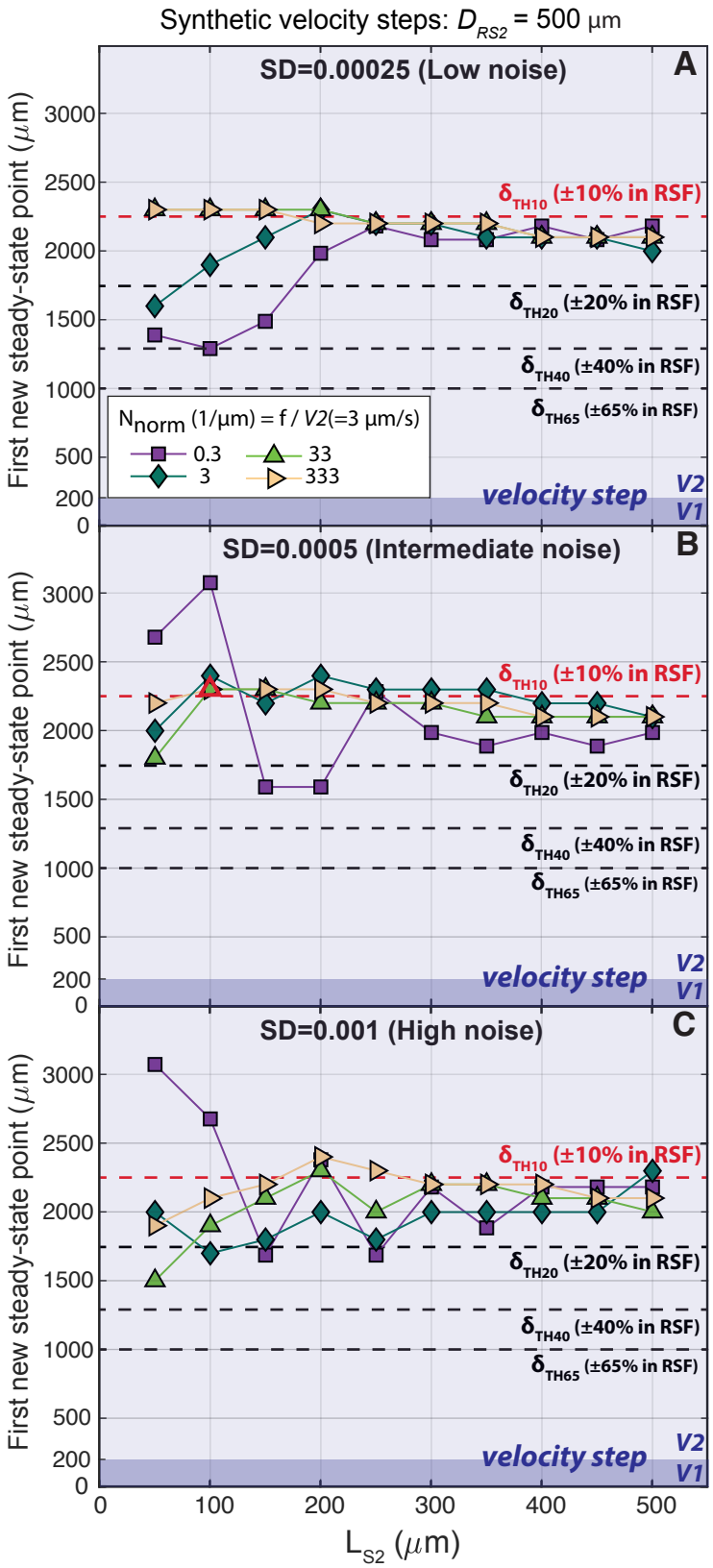

Figure 4. Compilation of outputs from the routine *steadystate*, reporting the first new steady-state (SS) points as a function of the slip-window length, L_{S2}. The SS analyses were conducted using the same synthetic friction velocity step (VS), which was generated multiple times at a wide range of random Gaussian noise levels of standard deviation (SD): (A) 0.00025, (B) 0.0005, and (C) 0.001, and numbers of points per unit displacement (N_{norm} ≈ 0.3, 3, 33, and 333 1/μm). Displacement at which the velocity step from V1 to V2 occurs is highlighted by the interface delimiting the two differently shaded regions in the graph. First new SS from VS with SD of 0.0005 and L_{S2} = 100 μm (red bordered triangle in part B) agrees well with the first SS point found using the nonautomated procedure followed in section 3 of the text, where the first new SS was found at displacements, $\delta = \delta_{TH10}$ (red dashed line). Region characterized by $\delta \geq \delta_{TH10}$ is expected to return rate-and-state friction parameters (RSF) within a ± 10% error, with $\delta \approx \delta_{TH10}$ being the ideal first new SS of this analysis; region with $\delta < \delta_{TH10}$ is associated with increasingly larger errors in fitted rate-and-state friction parameter values (quantified by δ_{TH20}, δ_{TH40}, and δ_{TH65}) compared to the intrinsic values toward lower displacements.

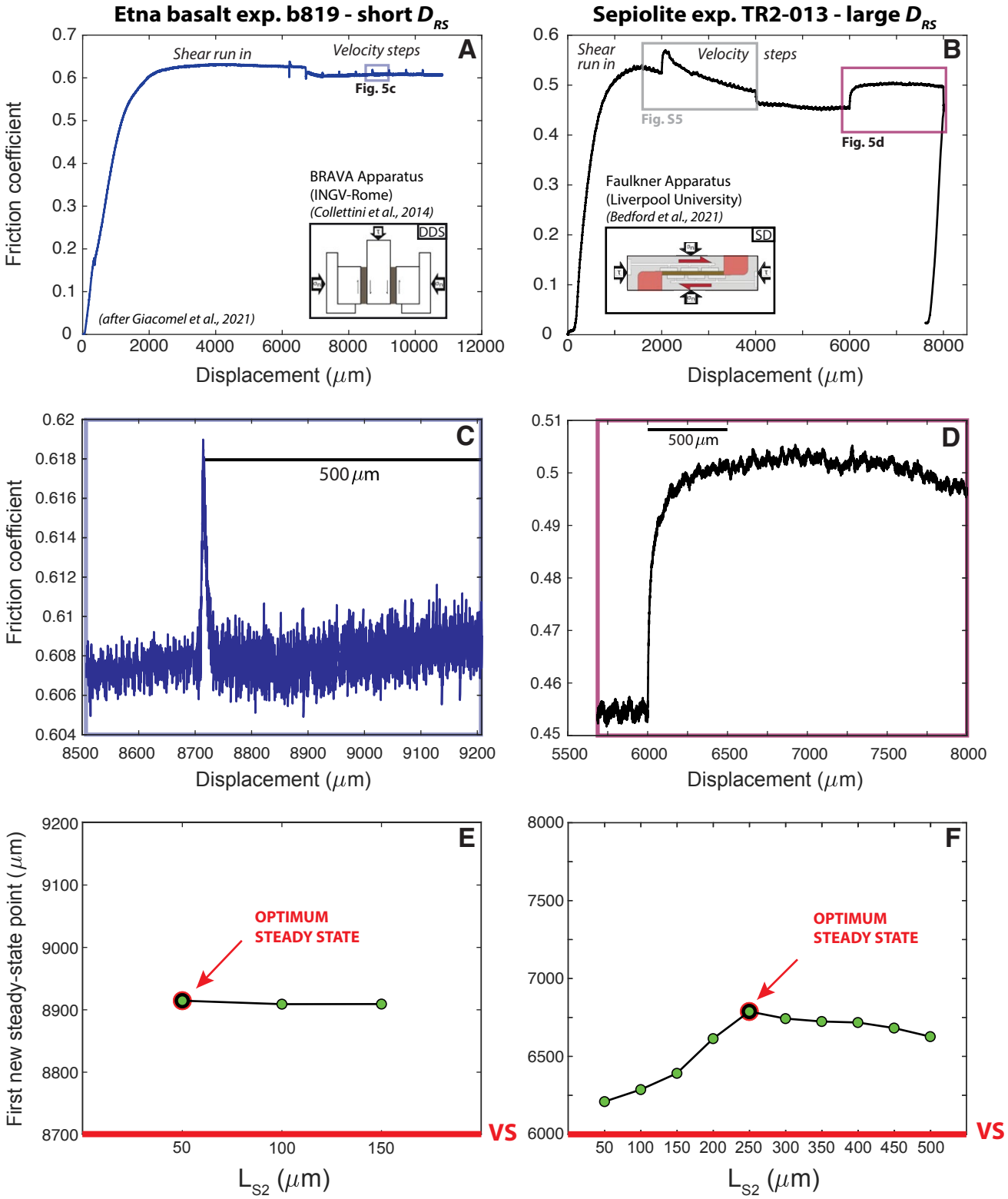

Figure 5. Friction tests were conducted using different simulated fault gouges with (A) short D_{RS} (Etna basalt) and (B) larger D_{RS} (sepiolite). DDS and SD acronyms denote double direct and single direct configurations used to run the experiments, respectively. (C and D) Selected velocity steps from such tests are magnified. (E and F) Collection of outputs from the two velocity steps using *steadystate*; the "optimum" first new steady-state point (green circle with red outline) with its associated slip window length L_{S2} is highlighted; bold red lines indicate the displacement at which the velocity step (VS) occurs.

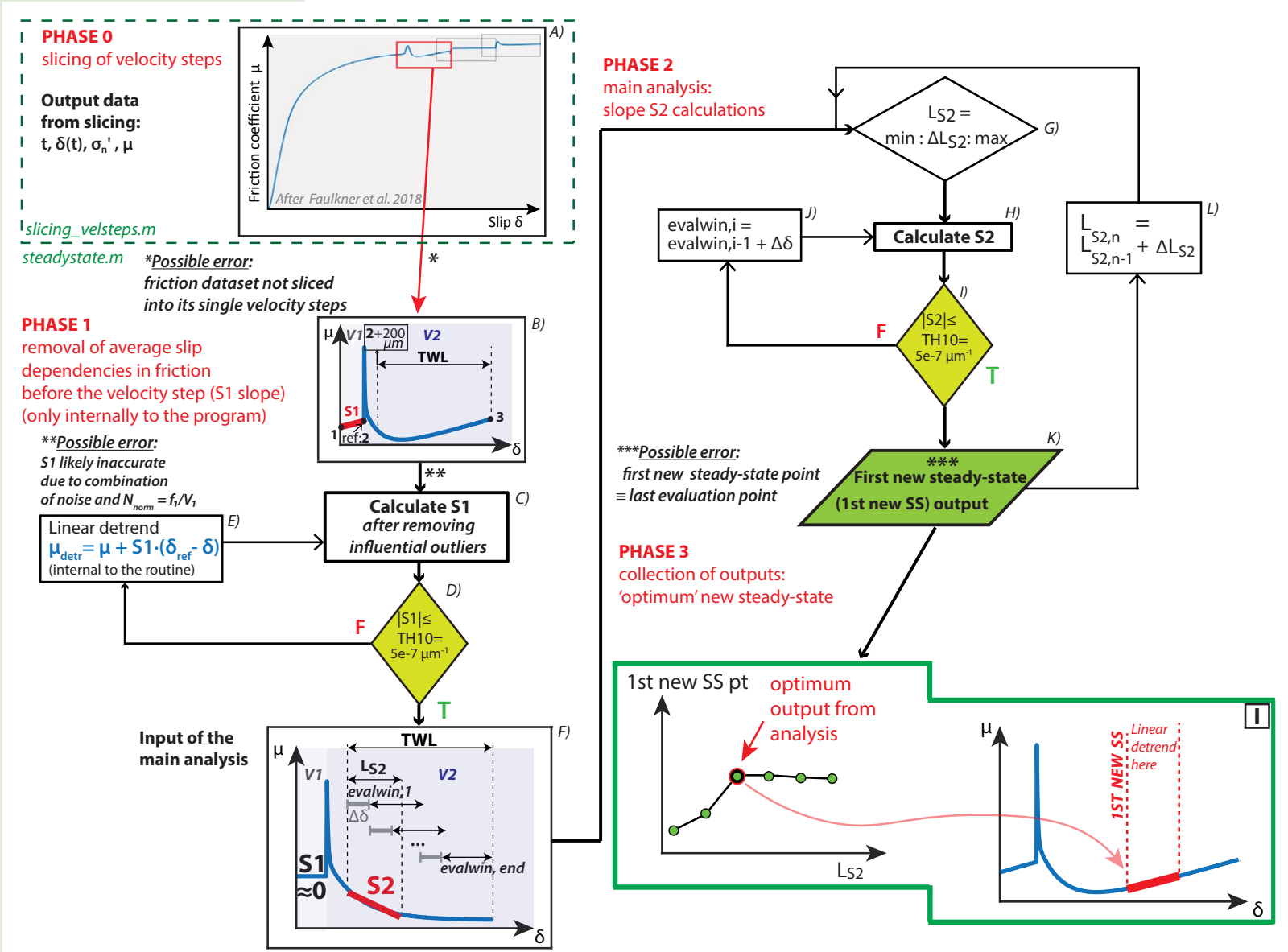

Figure 6. Flow chart describing the key steps (from A to L) followed by the routine *steadystate* to determine the first new steady-state (SS) point by systematically estimating S2 slopes within a range of S2 window lengths, L_{S2} (phase 2). Main SS routine is preceded by the slicing of the experimental data set into its single friction velocity steps (with slip-velocity steps from V1 to V2) through the script slicing_velstep (phase 0). For consistency in the determination of new SS conditions, average slope, S1, is internally removed in the script before the SS routine starts (phase 1). I represents the diagram summarizing the outputs of the routine, and specifically, the "optimum" pair of first new SS L_{S2} values (left) that need to be inputted to operate the linear detrend in the original velocity step (right) to retrieve rate-and-state friction parameters. Symbols and abbreviations: μ denotes the friction coefficient, and δ the displacement (in A and B); the numbers depicted in part B represent points selected by the user through *steadystate* before carrying out the automated SS friction analysis, in which S2 slopes can be estimated across the total window length (TWL); ref denotes the reference point upon the friction velocity step that needs to be inputted to remove the slope before the velocity step, S1 (in B and E); TH10 is the threshold numerically equivalent to $5 \cdot 10^{-7}$ μm^{-1}, below which the velocity step can be regarded as with null average trend of friction with slip when |S1| ≤ TH10 (part D, phase 1) and new SS conditions (= 1st new SS pt; in K and panel I) are achieved when |S2| ≈ S1 ≤ TH10 (in I, phase 2); $L_{S2,n}$ is the n-th length of the slip window used to calculate S2 (in F, G, and L), and evalwin,i is the i-th evaluation slip window of length L_{S2} that the routine uses to operate the linear regression to obtain S2 slopes (in F and J); Δδ is the amount of displacement by which evalwin is shifted from one iteration to the next (in F and J) until |S2| ≤ TH10 (in I); ΔL_{S2} represents the step increment of L_{S2} used for the next SS friction analysis, which is run from the minimum length, min, to the maximum length, max (in G and L).

points 1 and 2 (Fig. 6B) and compare these values with those obtained from a database of synthetic friction data with no overall slip dependencies in friction. This database is contained within *steadystate* to identify where linear regression may return an erratic S1 slope from the experiment, based on the combinations of noise level and N_{norm} that in the database return gradients $|S1| > 5 \times 10^{-7}$ μm^{-1}.

In the synthetic database, the average random noise is defined by the user in terms of random Gaussian noise with SD, while in experimental data sets the average noise levels are estimated in *steadystate* through the root mean square error (RMSE). RMSE is defined as the SD of the residuals, and is computed as:

$$\mathrm{RMSE} = \sqrt{\frac{\sum_{i=1}^{n}(y_i - \widehat{y_i})^2}{n-2}},$$

with y_i and $\widehat{y_i}$ denoting the i-th observed and predicted response, that in a friction-versus-displacement data set represent the i-th friction data point and the corresponding i-th friction value from the regression line, respectively, with *n*, the number of data points. This parameter is slope-independent an

$$\approx \mathrm{SD} = \sqrt{\frac{\sum_{i=1}^{n}(y_i - \bar{y})^2}{n-1}}$$

in data sets lacking any overall slip dependencies like those contained in the above database, given that in such cases the predicted responses ($\widehat{y_i}$) approach the estimated mean ($\bar{y}$). Satisfying the condition SD ≈ RMSE in our synthetic database thereby allows the comparison of the average noise values contained therein with those from the experimental data. Based on such analyses, an error ends the routine when the combination of the low number of data points and high noise level would probably produce inaccurate S1 estimates, and prompts the user to choose a wider slip window (L_{S1}). In the event that increasing L_{S1} may include data that are not considered steady state, additional velocity-stepping tests may be necessary with longer shear run-in stages or longer step lengths from the second velocity step onward.

To further address the possible presence of outliers introduced by the experimental noise, we determined the studentized residuals from a linear regression model. The studentized residual method is employed in statistics to eliminate outliers that influence the linear regression model to such an extent that the estimated regression function is "pulled" toward the potential outlier so that it is not flagged as an outlier using the classic standardized residual criterion. Such outliers have the potential to skew the regression line and influence the value of S1. A studentized residual is calculated by dividing the residual by an estimate of its standard deviation. More details can be found in Hastie et al. (2009), James et al. (2013), and Pardoe (2021). In *steadystate*, we define "influential outliers" as all of the studentized residuals with values outside of the ±3 bounds and run a linear regression devoid of these points to improve the accuracy of S1 determination (Fig. 6C).

5.3 Phase 2: Estimation of S2 Slopes

Phase 2 consists of multiple SS analyses that begin at 200 μm past the velocity jump (Fig. 6F), where the slope S2 is estimated within an evaluation slip window of a given fixed length, L_{S2} (Figs. 6F and 6J), which spans from the minimum L_{S2} ($\min\_L_{S2}$) to the maximum L_{S2} ($\max\_L_{S2}$) with step increments, ΔL_{S2}, from a new SS assessment to the next one (Figs. 6G and 6L).

In the framework of a single SS analysis, during each iteration, the absolute value of S2 is compared with TH10 = 5×10^{-7} μm^{-1} (Fig. 2). If |S2| > TH10, a new linear regression is run, adding on net slip increments, Δδ, to produce a new starting point to determine S2 (Figs. 6F and 6H). The iterations stop once |S2| ≤ TH10 is satisfied, or until the end of the datafile is reached if such a criterion is not met. The displacement at which iterations stop is recorded as the first new SS point associated with a given L_{S2} (Fig. 6K; panel I, left side, Fig. 6). When the last datapoint is reached, a warning is given; at the second warning of the same type, an error ends the routine with the suggestion that a repeat test with longer VSs may be required to address the issue.

To conduct phase 2, four input parameters (in microns) are required in *steadystate* in the following order: $\min\_L_{S2}$, $\max\_L_{S2}$, ΔL_{S2}, and Δδ. In the first instance, the parameters should be left blank or null (i.e., []). In this case, the routine uses its default settings that for $\min\_L_{S2}$ and ΔL_{S2} amount to 50 μm, and calculates Δδ, which is numerically equivalent to the slip distance between two datapoints from point 2 + 200 μm onwards. If the net slip increment, Δδ, is overridden by the user, a warning sign appears if the entered value is lower than the displacement between datapoints, resulting in the replacement of the former value with the default argument to continue the analysis. $\max\_L_{S2}$ is a function of the total window length (TWL), which is defined as between point 2 + 200 μm and point 3 (Figs. 6B and 6F). When TWL ≤ 1000 μm, $\max\_L_{S2}$ equals 50% of TWL being approximated to the closest multiple of 100, whereas if TWL > 1000 μm, $\max\_L_{S2}$ is limited to 500 μm. This $\max\_L_{S2}$ upper boundary is aimed at limiting the proportion of frictional transients in S2 calculations, which may result in new SS detection at smaller displacements than true SS.

When the three arguments associated with L_{S2} are inputted by the user, the routine first approximates ΔL_{S2} to the closest multiple of 10 and according to the input arguments, it rounds $\min\_L_{S2}$ and $\max\_L_{S2}$ to the closest multiple of the approximated ΔL_{S2}. Moreover, in the MATLAB command window, *steadystate* suggests an optimal value for $\max\_L_{S2}$ following the same criteria used for the default settings.

5.4 Phase 3: Collection and Checking of Outputs: Optimum New Steady State

At the end of the routine, the collection of displacement values corresponding to new SS, namely the first new SS points, is plotted against their corresponding S2 window lengths (L_{S2}), where the optimum SS output is

highlighted. The optimum choice of the first new SS point is the displacement value coupled with the smallest L_{S2}, pertaining to the approximately constant portion of the plot (Fig. 6, left side, panel I). These values should then be used for linear detrending of the VS (Fig. 6, right side, panel I). The routine also provides the user with the opportunity to save outputs in Excel format.

Following on the output generation from the SS analysis, although unlikely, there is a slight possibility that the routine returns no optimum outputs from the SS analysis. This may occur as a result of highly scattered first new SS values as a function of L_{S2}, in data sets characterized by significant noise and a low-number of data points, despite adopting a wide range of L_{S2}. In this case, the routine quits with an associated error, as proceeding with the linear detrend and the inversion for the RSF parameters is not recommended. Such an error is followed by the suggestion to either attempt repeating the SS analysis with a larger max_L_{S2} (of the amount ΔL_{S2}), or to run another velocity-stepping test with a larger number of points per unit slip.

6. CONCLUDING REMARKS

We present the case for ensuring proper identification of steady-state conditions when processing laboratory friction data to estimate RSF parameters. We show from the processing of synthetic data sets that serious discrepancies between the modeled and intrinsic RSF parameters can result from the processing of data where steady-state is incorrectly identified. To address these issues, we introduce a methodology to identify steady-state conditions based on the achievement of similar slopes before and after a velocity step.

The methodology has been developed into a MATLAB-based routine called *steadystate* to produce unbiased, consistent, and reliable determination of new steady-state conditions under a broad range of experimental conditions and sheared materials. We hope that this will promote progress toward consistent parameter estimation techniques and reduce reliance on arbitrary user-dependent choices of steady-state during the processing of laboratory friction data that can lead to notable discrepancies in RSF parameter estimation from the same data set.

Our systematic analysis of synthetic data sets emphasizes that slope estimations and, consequently, new steady-state determinations, can be negatively affected by high-noise levels and a low-number of points per unit slip of friction data, given the same intrinsic RSF properties of the material (Fig. 4). We show how these problems can be circumvented by systematically evaluating a range of slip-window lengths (L_{S2}) when assessing new steady-state conditions. The routine not only identifies the first displacement at which steady-state conditions are achieved, it provides the minimum evaluation window length (L_{S2}) it used to determine this point. These two values can then be used to linearly detrend the friction data, and thus, to accurately determine the RSF parameters.

Following the identification of an accurate first steady-state point, coupled with a sufficiently large L_{S2} to produce a good linear detrend, it is good practice to first perform a two-state variable fit, and replace it with a one-state variable model only if RSF parameter values degenerate into a one-state variable fit (i.e., $b_2 \approx 0$ or $D_{RS1} \approx D_{RS2}$). This protocol is motivated by the observation that a one-state variable fit fails to describe the friction evolution with slip if the velocity step obeys a two-state variable constitutive law (Figs. 2B and 2D).

This study confirms that materials characterized by long frictional transients with slip after velocity steps, such as clays (Fig. 5D), often require larger displacements to attain new steady-state conditions when compared to the step length of 500 µm that is typically used in velocity-stepping tests (Fig. 5F). Under such circumstances, modeled RSF parameter values would significantly depart from the true values if the intrinsic D_{RS2} were commensurate with the whole displacement window that contains the velocity step. Conversely, in materials with short frictional transients with slip following the velocity jumps (Fig. 5C), running velocity steps with 500 µm step length is normally sufficient to determine new steady-state (Fig. 5E). Furthermore, in these materials, since RSF estimates are less sensitive to the accuracy of steady-state determination (Fig. 3), operating the detrend "by eye," as has been done routinely so far, would still likely produce good RSF fits.

These observations suggest that further investigation is warranted to better decipher the nature of the two-state variable, which is currently used to produce better RSF fits in long-evolution velocity steps, but whose underlying physical significance is still largely unknown.

Finally, to date, *steadystate* has been purposely designed to work in conjunction with an RSF modeling technique. However, its applicability in the future could be expanded to any situation involving a general slope estimation (e.g., calculating the elastic moduli, any linear slip dependence in friction, etc.).

ACKNOWLEDGMENTS

P. Giacomel and D.R. Faulkner gratefully acknowledge Natural Environment Research Council grant NE/V011804/1 for funding this work. Reviewers R. Skarbek and M. Ikari are warmly thanked for their insightful comments and suggestions that further improved this work. R. Skarbek is greatly thanked for providing the MATLAB spring-slider model for generation of synthetic velocity steps. M. Dalla Pria is gratefully acknowledged for his suggestions on inferential statistics, and M. Battaglia is thanked for his advice on coding. M. Ikari and A.M. Eijsink are warmly thanked for providing experimental data from MARUM Laboratory to test the code. This work also benefited from insightful discussions with E. Mariani, I. Ashman, and L. Xi.

REFERENCES CITED

Agliardi, F., Scuderi, M.M., Fusi, N., and Collettini, C., 2020, Slow-to-fast transition of giant creeping rockslides modulated by undrained loading in basal shear zones: Nature Communications, v. 11, no. 1, 1352, https://doi.org/10.1038/s41467-020-15093-3.

Bedford, J.D., Faulkner, D.R., Allen, M.J., and Hirose, T., 2021, The stabilizing effect of high pore-fluid pressure along subduction megathrust faults: Evidence from friction experiments on accretionary sediments from the Nankai Trough: Earth and Planetary Science Letters, v. 574, https://doi.org/10.1016/j.epsl.2021.117161.

Bhattacharya, P., Rubin, A.M., Bayart, E., Savage, H.M., and Marone, C., 2015, Critical evaluation of state evolution laws in rate and state friction: Fitting large velocity steps in simulated fault gouge with time-, slip-, and stress-dependent constitutive laws: Journal of Geophysical Research: Solid Earth, v. 120, no. 9, p. 6365–6385, https://doi.org/10.1002/2015JB012437.

Blanpied, M., Marone, C., Lockner, D., Byerlee, J., and King, D., 1998, Quantitative measure of the variation in fault rheology due to fluid-rock interactions: Journal of Geophysical Research: Solid Earth, v. 103, no. B5, p. 9691–9712, https://doi.org/10.1029/98JB00162.

Chartrand, R., 2011, Numerical differentiation of noisy, nonsmooth data: International Scholarly Research Notices, v. 2011, https://doi.org/10.5402/2011/164564.
Collettini, C., Di Stefano, G., Carpenter, B., Scarlato, P., Tesei, T., Mollo, S., Trippetta, F., Marone, C., Romeo, G., and Chiaraluce, L., 2014, A novel and versatile apparatus for brittle rock deformation: International Journal of Rock Mechanics and Mining Sciences, v. 66, p. 114–123, https://doi.org/10.1016/j.ijrmms.2013.12.005.
Cook, N.G., 1981, Stiff testing machines, stick slip sliding, and the stability of rock deformation, *in* Carter, N.L., Friedman, C.M., Logan, J.M., and Stearns, D.W., eds., Mechanical Behavior of Crustal Rocks: The Handin Volume: American Geophysical Union, Geophysical Monograph Series, v. 24, p. 93–102.
Dal Zilio, L., Lapusta, N., Avouac, J.-P., and Gerya, T., 2022, Subduction earthquake sequences in a non-linear visco-elasto-plastic megathrust: Geophysical Journal International, v. 229, no. 2, p. 1098–1121, https://doi.org/10.1093/gji/ggab521.
Dieterich, J.H., 1979, Modeling of rock friction: 1. Experimental results and constitutive equations: Journal of Geophysical Research: Solid Earth, v. 84, no. B5, p. 2161–2168, https://doi.org/10.1029/JB084iB05p02161.
Dieterich, J.H., 1981, Constitutive properties of faults with simulated gouge: Mechanical behavior of crustal rocks, *in* Carter, N.L., Friedman, C.M., Logan, J.M., and Stearns, D.W., eds., Mechanical Behavior of Crustal Rocks: The Handin Volume: American Geophysical Union, Geophysical Monograph Series, v. 24, p. 103–120.
Dieterich, J.H., 1992, Earthquake nucleation on faults with rate-and state-dependent strength: Tectonophysics, v. 211, no. 1–4, p. 115–134, https://doi.org/10.1016/0040-1951(92)90055-B.
Dieterich, J.H., and Conrad, G., 1984, Effect of humidity on time-and velocity-dependent friction in rocks: Journal of Geophysical Research: Solid Earth, v. 89, no. B6, p. 4196–4202, https://doi.org/10.1029/JB089iB06p04196.
Erickson, B.A., et al., 2023, Incorporating full elastodynamic effects and dipping fault geometries in community code verification exercises for Simulations of Earthquake Sequences and Aseismic Slip (SEAS): Bulletin of the Seismological Society of America, v. 113, no. 2, p. 499–523, https://doi.org/10.1785/0120220066.
Faulkner, D.R., Sanchez-Roa, C., Boulton, C., and Den Hartog, S., 2018, Pore fluid pressure development in compacting fault gouge in theory, experiments, and nature: Journal of Geophysical Research: Solid Earth, v. 123, no. 1, p. 226–241, https://doi.org/10.1002/2017JB015130.
Frank, F., 1965, On dilatancy in relation to seismic sources: Reviews of Geophysics, v. 3, no. 4, p. 485–503, https://doi.org/10.1029/RG003i004p00485.
Giacomel, P., Ruggieri, R., Scuderi, M.M., Spagnuolo, E., Di Toro, G., and Collettini, C., 2021, Frictional properties of basalt experimental faults and implications for volcano-tectonic settings and geo-energy sites: Tectonophysics, v. 811, https://doi.org/10.1016/j.tecto.2021.228883.
Giorgetti, C., Carpenter, B.M., and Collettini, C., 2015, Frictional behavior of talc-calcite mixtures: Journal of Geophysical Research: Solid Earth, v. 120, no. 9, p. 6614–6633, https://doi.org/10.1002/2015JB011970.
Goldsby, D.L., Rar, A., Pharr, G.M., and Tullis, T.E., 2004, Nanoindentation creep of quartz, with implications for rate- and state-variable friction laws relevant to earthquake mechanics: Journal of Materials Research, v. 19, no. 1, p. 357–365, https://doi.org/10.1557/jmr.2004.19.1.357.
Gu, J.-C., Rice, J.R., Ruina, A.L., and Simon, T.T., 1984, Slip motion and stability of a single degree of freedom elastic system with rate and state dependent friction: Journal of the Mechanics and Physics of Solids, v. 32, no. 3, p. 167–196, https://doi.org/10.1016/0022-5096(84)90007-3.
Handwerger, A.L., Rempel, A.W., Skarbek, R.M., Roering, J.J., and Hilley, G.E., 2016, Rate-weakening friction characterizes both slow sliding and catastrophic failure of landslides: Proceedings of the National Academy of Sciences of the United States of America, v. 113, no. 37, p. 10,281–10,286, https://doi.org/10.1073/pnas.1607009113.
Hastie, T., Tibshirani, R., Friedman, J.H., and Friedman, J.H., 2009, The Elements of Statistical Learning: Data Mining, Inference, and Prediction: Springer, 745 p., https://doi.org/10.1007/978-0-387-84858-7.
Helmstetter, A., Sornette, D., Grasso, J.R., Andersen, J.V., Gluzman, S., and Pisarenko, V., 2004, Slider block friction model for landslides: Application to Vaiont and La Clapiere landslides: Journal of Geophysical Research: Solid Earth, v. 109, https://doi.org/10.1029/2002JB002160.
Hudson, T.S., Kufner, S.K., Brisbourne, A.M., Kendall, J.M., Smith, A.M., Alley, R.B., Arthern, R.J., and Murray, T., 2023, Highly variable friction and slip observed at Antarctic ice stream bed: Nature Geoscience, v. 16, no. 7, p. 612–618, https://doi.org/10.1038/s41561-023-01204-4.
Ikari, M.J., 2019, Laboratory slow slip events in natural geological materials: Geophysical Journal International, v. 218, no. 1, p. 354–387, https://doi.org/10.1093/gji/ggz143.
Ikari, M.J., and Hüpers, A., 2021, Velocity-weakening friction induced by laboratory-controlled lithification: Earth and Planetary Science Letters, v. 554, https://doi.org/10.1016/j.epsl.2020.116682.
Ito, Y., and Ikari, M.J., 2015, Velocity-and slip-dependent weakening in simulated fault gouge: Implications for multimode fault slip: Geophysical Research Letters, v. 42, no. 21, p. 9247–9254, https://doi.org/10.1002/2015GL065829.
James, G., Witten, D., Hastie, T., and Tibshirani, R., 2013, An Introduction to Statistical Learning: Springer, https://doi.org/10.1007/978-1-4614-7138-7.
Kilgore, B.D., Blanpied, M.L., and Dieterich, J.H., 1993, Velocity dependent friction of granite over a wide range of conditions: Geophysical Research Letters, v. 20, no. 10, p. 903–906, https://doi.org/10.1029/93GL00368.
Lambert, V., Lapusta, N., and Faulkner, D., 2021, Scale dependence of earthquake rupture prestress in models with enhanced weakening: Implications for event statistics and inferences of fault stress: Journal of Geophysical Research: Solid Earth, v. 126, no. 10, https://doi.org/10.1029/2021JB021886.
Leeman, J.R., Saffer, D.M., Scuderi, M.M., and Marone, C., 2016, Laboratory observations of slow earthquakes and the spectrum of tectonic fault slip modes: Nature Communications, v. 7, no. 1, https://doi.org/10.1038/ncomms11104.
Marone, C., 1998, Laboratory-derived friction laws and their application to seismic faulting: Annual Review of Earth and Planetary Sciences, v. 26, no. 1, p. 643–696, https://doi.org/10.1146/annurev.earth.26.1.643.
Marone, C., and Cox, S., 1994, Scaling of rock friction constitutive parameters: The effects of surface roughness and cumulative offset on friction of gabbro: Pure and Applied Geophysics, v. 143, p. 359–385, https://doi.org/10.1007/BF00874335.
Marone, C., Raleigh, C.B., and Scholz, C., 1990, Frictional behavior and constitutive modeling of simulated fault gouge: Journal of Geophysical Research: Solid Earth, v. 95, no. B5, p. 7007–7025, https://doi.org/10.1029/JB095iB05p07007.
McCarthy, C., Savage, H., and Nettles, M., 2017, Temperature dependence of ice-on-rock friction at realistic glacier conditions: Philosophical Transactions, Series A: Mathematical, Physical and Engineering Sciences, v. 375, no. 2086, https://doi.org/10.1098/rsta.2015.0348.
Nakatani, M., 2001, Conceptual and physical clarification of rate and state friction: Frictional sliding as a thermally activated rheology: Journal of Geophysical Research: Solid Earth, v. 106, no. B7, p. 13,347–13,380, https://doi.org/10.1029/2000JB900453.
Niemeijer, A., Marone, C., and Elsworth, D., 2010, Frictional strength and strain weakening in simulated fault gouge: Competition between geometrical weakening and chemical strengthening: Journal of Geophysical Research: Solid Earth, v. 115, no. B10, https://doi.org/10.1029/2009JB000838.
Noda, H., and Shimamoto, T., 2009, Constitutive properties of clayey fault gouge from the Hanaore fault zone, southwest Japan: Journal of Geophysical Research: Solid Earth, v. 114, https://doi.org/10.1029/2008JB005683.
Pardoe, I., 2021, Applied Regression Modeling: Hoboken, New Jersey, John Wiley & Sons, 310 p., https://doi.org/10.1002/9781119615941.
Pozzi, G., Collettini, C., Scuderi, M.M., Tesei, T., Marone, C., Amodio, A., and Cocco, M., 2023, Fabric controls fault stability in serpentinite gouges: Geophysical Journal International, v. 235, no. 2, p. 1778–1797, https://doi.org/10.1093/gji/ggad322.
Reinen, L.A., and Weeks, J.D., 1993, Determination of rock friction constitutive parameters using an iterative least squares inversion method: Journal of Geophysical Research: Solid Earth, v. 98, no. B9, p. 15,937–15,950, https://doi.org/10.1029/93JB00780.
Rice, J.R., and Ruina, A.L., 1983, Stability of steady frictional slipping: Journal of Applied Mechanics, v. 50, no. 2, p. 343–349, https://doi.org/10.1115/1.3167042.
Rubin, A.M., 2008, Episodic slow slip events and rate-and-state friction: Journal of Geophysical Research: Solid Earth, v. 113, no. B11, https://doi.org/10.1029/2008JB005642.
Rubin, A.M., and Ampuero, J.P., 2005, Earthquake nucleation on (aging) rate and state faults: Journal of Geophysical Research: Solid Earth, v. 110, https://doi.org/10.1029/2005JB003686.
Ruggieri, R., Scuderi, M.M., Trippetta, F., Tinti, E., Brignoli, M., Mantica, S., Petroselli, S., Osculati, L., Volontè, G., and Collettini, C., 2021, The role of shale content and pore-water saturation on frictional properties of simulated carbonate faults: Tectonophysics, v. 807, https://doi.org/10.1016/j.tecto.2021.228811.
Ruina, A., 1983, Slip instability and state variable friction laws: Journal of Geophysical Research: Solid Earth, v. 88, no. B12, p. 10,359–10,370, https://doi.org/10.1029/JB088iB12p10359.

Sánchez-Roa, C., Jiménez-Millán, J., Abad, I., Faulkner, D.R., Nieto, F., and García-Tortosa, F.J., 2016, Fibrous clay mineral authigenesis induced by fluid-rock interaction in the Galera fault zone (Betic Cordillera, SE Spain) and its influence on fault gouge frictional properties: Applied Clay Science, v. 134, p. 275–288, https://doi.org/10.1016/j.clay.2016.06.023.

Sánchez-Roa, C., Faulkner, D., Boulton, C., Jimenez-Millan, J., and Nieto, F., 2017, How phyllosilicate mineral structure affects fault strength in Mg-rich fault systems: Geophysical Research Letters, v. 44, no. 11, p. 5457–5467, https://doi.org/10.1002/2017GL073055.

Sawai, M., Niemeijer, A.R., Plümper, O., Hirose, T., and Spiers, C.J., 2016, Nucleation of frictional instability caused by fluid pressurization in subducted blueschist: Geophysical Research Letters, v. 43, no. 6, p. 2543–2551, https://doi.org/10.1002/2015GL067569.

Scholz, C.H., 2019, The Mechanics of Earthquakes and Faulting: Cambridge, UK, Cambridge University Press, 519 p., https://doi.org/10.1017/9781316681473.

Scuderi, M.M., Collettini, C., Viti, C., Tinti, E., and Marone, C., 2017, Evolution of shear fabric in granular fault gouge from stable sliding to stick slip and implications for fault slip mode: Geology, v. 45, no. 8, p. 731–734, https://doi.org/10.1130/G39033.1.

Shroff, S.S., Ansari, N., Robert Ashurst, W., and de Boer, M.P., 2014, Rate-state friction in microelectromechanical systems interfaces: Experiment and theory: Journal of Applied Physics, v. 116, 244902, https://doi.org/10.1063/1.4904060.

Skarbek, R.M., and Savage, H.M., 2019, RSFit3000: A MATLAB GUI-based program for determining rate and state frictional parameters from experimental data: Geosphere, v. 15, no. 5, p. 1665–1676, https://doi.org/10.1130/GES02122.1.

Terzaghi, K., 1925, The Mechanics of Earth Construction Based on Soil Physics, translated from German: F. Deuticke [in German].

Thom, C.A., Hansen, L.N., Goldsby, D.L., and Brodsky, E.E., 2023, A microphysical model of rock friction and the brittle-ductile transition controlled by dislocation glide and backstress evolution: Journal of Geophysical Research: Solid Earth, v. 128, no. 2, https://doi.org/10.1029/2022JB024150.

Zoet, L., Carpenter, B., Scuderi, M., Alley, R., Anandakrishnan, S., Marone, C., and Jackson, M., 2013, The effects of entrained debris on the basal sliding stability of a glacier: Journal of Geophysical Research: Earth Surface, v. 118, no. 2, p. 656–666, https://doi.org/10.1002/jgrf.20052.